Available online at www.sciencedirect.com

ScienceDirect

Procedia Social and Behavioral Sciences 17 (2011) 678–697

Procedia
Social and Behavioral Sciences

19th International Symposium on Transportation and Traffic Theory

Characterization of Traffic Oscillation Propagation under Nonlinear Car-Following Laws

Xiaopeng Li and Yanfeng Ouyang[1]

Department of Civil and Environmental Engineering
University of Illinois at Urbana-Champaign, Urbana, IL 61801

Abstract

Unlike linear car-following models, nonlinear models generally can generate more realistic traffic oscillation phenomenon, but nonlinearity makes analytical quantification of oscillation characteristics (e.g, periodicity and amplitude) significantly more difficult. This paper proposes a novel mathematical framework that accurately quantifies oscillation characteristics for a general class of nonlinear car-following laws. This framework builds on the describing function technique from nonlinear control theory and is comprised of three modules: expression of car-following models in terms of oscillation components, analyses of local and asymptotic stabilities, and quantification of oscillation propagation characteristics. Numerical experiments with a range of well-known nonlinear car-following laws show that the proposed approach is capable of accurately predicting oscillation characteristics under realistic physical constraints and complex driving behaviors. This framework not only helps further understand the root causes of the traffic oscillation phenomenon but also paves a solid foundation for the design and calibration of realistic nonlinear car-following models that can reproduce empirical oscillation characteristics.

Keywords: Traffic oscillation; Describing function; Nonlinear; Car-following law

1. Introduction

Traffic oscillations, also known as the "stop-and-go" traffic, refer to the phenomenon that vehicle movement in congested traffic tends to alternate cyclically between "stop" (or slow movements) and "go" (or fast movements) patterns. Traffic oscillations lead to a range of adverse consequences including safety hazards, travel delay, extra fuel consumption, air pollution and driving discomfort. In the 1980s, empirical studies used loop detector data as solid evidences of periodically oscillating patterns in congested traffic [1, 2, 3]. Later, in the synchronized flow context [4, 5, 6], Helbing et al. [7] and Kerner [8] categorized observed oscillations into different patterns. Methods to extract oscillation characteristics (e.g., frequency and amplitude) from traffic data have been proposed in the time domain [9, 10, 11] and the frequency domain [12]. Empirical studies have also related traffic oscillations to highway capacity drops [13, 14, 15], lane changes near merges and diverges [10, 15, 16, 17, 18, 19, 20], and roadway geometric features [21].

Motivated by these empirical findings, intensive theoretical research has been conducted to investigate oscillation formation and propagation mechanisms. Early studies on linear car-following models can be traced back to the 1950s

[1]Corresponding author. Tel.: 217-333-9858, E-mail: yfouyang@illinois.edu.

1877–0428
doi:10.1016/j.sbspro.2011.04.538

[22, 23]. Later, various non-linear models (e.g., [24, 25]) were developed in hope to better reproduce traffic evolution. For example, Bando et al. ([26, 27]) developed a nonlinear optimal velocity (OV) model to study the stop-and-go traffic, which became the building block of a set of extended models [28, 29, 30, 31, 32]. Treiber et al. [33] proposed an intelligent driver model (IDM) to qualitatively reproduce observed traffic oscillations on German freeways. The IDM model has been revisited in a number of following studies, e.g., relating it to a macroscopic model [34] and adjusting it to match observed patterns in more data sets [35, 36].

In spite of numerous attempts, however, few car-following models are able to quantitatively explain propagation mechanisms of the observed traffic oscillation phenomenon. Although the oscillation behavior of linear car-following models can be easily analyzed by frequency-domain analysis tools [22, 23], the results have very limited capabilities of explaining real-world traffic oscillation evolution, primarily because of its exclusion of physical constraints (e.g., speed bounds) and nonlinear driving behaviors. For example, without imposing speed bounds, the magnitude of oscillation may grow to infinity at an exponential rate. The hope for a better explanation of the stop-and-go phenomenon lies on the development of more complex nonlinear car-following models. For example, recent studies that try to explain oscillation propagation with nonlinear car-following behavior include [37, 38, 39, 40, 41, 42, 43, 44]. See [45] for a comprehensive review on this topic. However, due to the complexity from nonlinearity, these studies are mainly based on either numerical simulations or linearization of models. It remains a challenge to analytically quantify the global oscillation propagation properties of nonlinear car-following models. Without a clear connection between the car-following models' structure (and parameter setting) and their oscillation behavior, it is generally very difficult to calibrate a suitable car-following model that matches the observed oscillation characteristics.

This paper aims to fill some of these gaps by proposing a mathematical approach that, for the first time, can analytically quantify oscillation characteristics of general nonlinear car-following laws based on frequency response of nonlinear systems. This framework starts with a novel transformation scheme that expresses a general car following law in terms of pure oscillation components. Then the describing function technique from nonlinear control theory [46, 47] is applied to analyze the local and asymptotic stability properties and the propagation of oscillations. This technique approximates the output of a nonlinear system by the fundamental frequency component (which is computationally easy to characterize), and it allows us to derive a compact frequency response function of a nonlinear car-following law. We illustrate the application of this analytical framework with a set of nonlinear car-following laws, and the analytical predictions are compared with the results from numerical simulations. Numerical experiments show that the proposed method provides an accurate prediction of oscillation propagation in a vehicle platoon. The proposed framework can potentially enable the development of a guideline for designing and calibrating car-following models that can reproduce empirically observed oscillation characteristics.

The remainder of the paper has the following structure. Section 2 introduces notation and proposes a new formulation scheme that expresses a general class of car-following laws in terms of pure oscillation components. Section 3 describes the analytical mathematical framework, including the nonlinear car-following stability analysis and oscillation propagation quantification. Section 4 illustrates the application of this framework to a number of well-known car-following models; the performance of the proposed method is examined with numerical examples. Section 5 concludes this paper and briefly discusses possible future research directions.

2. Car-following Law Representation

Generally, vehicle trajectories exhibit both macroscopic and microscopic characteristics. Macroscopic characteristics are specified by nominal states (e.g., average spacing, velocity and flow volume) that shall be consistent with a traffic fundamental diagram [48]. Microscopic characteristics describe how actual vehicle trajectories deviate from the nominal states as a result of car-following dynamics, and such characteristics can often be approximately specified by oscillation properties (e.g., period and amplitude). The coupled oscillation and nominal state components make it difficult to analyze and quantify traffic oscillation properties. Inspired by the "detrending" operations in traffic and supply chain analysis (e.g., [12, 49]), this section proposes a decomposition method that extracts pure oscillation components from vehicle trajectories, which further allows us to represent a general class of non-linear car-following models in terms of only oscillation components. As such, the interference from nominal states is eliminated.

2.1. Trajectory decomposition

As shown in Figure 1, we consider a platoon of vehicles in a single lane, $l = 0, 1, ..., L$, indexed from downstream to upstream. In an infinite time horizon $t \in \mathbb{R}$, let $x_l(t) \in \mathbb{R}$ denotes the location of vehicle l at time t. The actual trajectory of vehicle l can be denoted by a curve $\mathbf{x}_l = \{x_l(t)\}_{t\in\mathbb{R}}$.[2] Since vehicles normally do not move backwards, $x_l(t)$ shall be monotonically non-decreasing with t.

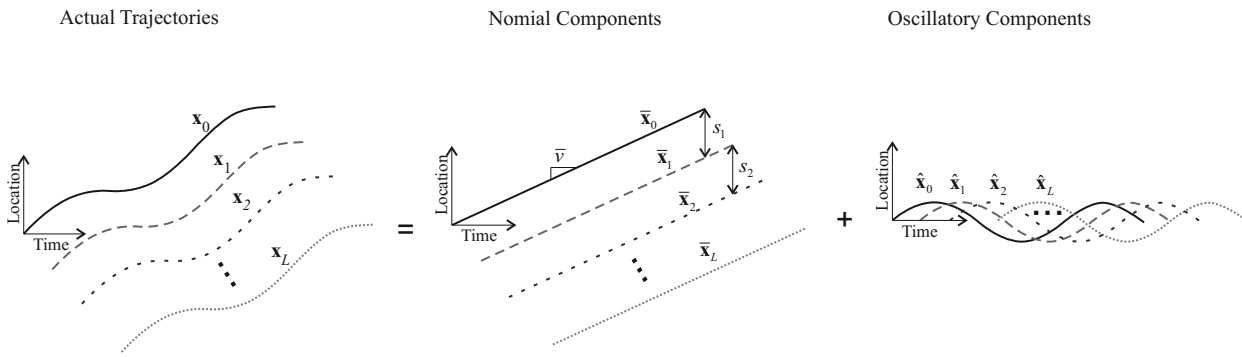

Figure 1: Decomposition of trajectories

Definition 1. We call $\mathbf{y} = \{y(t)\}_{t\in\mathbb{R}}$ *an oscillatory time series* if $\exists P \in \mathbb{R}_+, -\infty < y(t) = y(t+P) < +\infty, \forall t \in \mathbb{R}$ and $\int_0^P y(t) = 0$, or equivalently $\mathbf{y}$ is comprised of a set of sinusoids (or frequency components) whose frequencies are all multiples of $2\pi/P$.

Definition 2. We say that a time series contains *periodic patterns* if it is a superposition of a time series of nominal states (which represents the trend) and an oscillatory time series (which captures oscillations).

Definition 3. For two given time series $\mathbf{y}_1 := \{y_1(t)\}_{t\in\mathbb{R}}$ and $\mathbf{y}_2 := \{y_2(t)\}_{t\in\mathbb{R}}$, their *difference* is defined as $\mathbf{y}_1 - \mathbf{y}_2 := \{y_1(t) - y_2(t)\}_{t\in\mathbb{R}}$.

[12] observed that a vehicle trajectory with well-developed oscillations demonstrates very salient periodicity and can be approximated by a narrow band of frequency components after detrending (i.e., removing the nominal series). As illustrated in Figure 1, we assume that trajectory $\mathbf{x}_l$ is a superposition of a nominal series $\bar{\mathbf{x}}_l = \{\bar{x}_l(t)\}_{t\in\mathbb{R}}$ that dictates the underlying macroscopic traffic characteristics (e.g, trend speed and average spacing) and an oscillatory series $\hat{\mathbf{x}}_l = \{\hat{x}_l(t)\}_{t\in\mathbb{R}}$ that results from car-following dynamics. Since the macroscopic characteristics of vehicle trajectories usually remain relatively stable in a short period of time, the linear regression line of a trajectory could potentially be considered as its nominal series[3] and the remaining components (i.e., by subtracting the nominal series from the original trajectory) can be treated as the oscillatory part. In general, we use the average speed $\bar{v}$ and a set of average spacings $\{s_l\}_{\forall l}$ (i.e., $s_l := \bar{x}_{l-1}(t) - \bar{x}_l(t), \forall t$) to denote the macroscopic characteristics. For each vehicle l, $\bar{x}_l(t) = \bar{x}_0(0) + \bar{v}t - \sum_{l'=1}^{l} s_{l'}$ and hence $\hat{x}_l(t)$ satisfies

$$\hat{x}_l(t) = x_l(t) - \bar{x}_0(0) - \bar{v}t + \sum_{l'=1}^{l} s_{l'}, \forall t \in \mathbb{R}, l = 0, 1, \cdots, L. \tag{1}$$

Even for non-stationary traffic where macroscopic characteristics vary over time (e.g., transition from a free-flow state to a congestion state), the macroscopic characteristics usually have a much slower evolving pace than traffic oscillations. The above-mentioned decomposition scheme can be easily adapted to handle such cases by allowing $\{\bar{\mathbf{x}}_l\}_{\forall l}$ to be non-stationary but slowly varying. The other decomposition steps remain unchanged.

[2] A realistic trajectory with finite length can be transformed into an infinite trajectory by padding its own copies or zeros.

[3] In case the macroscopic characteristics vary along the trajectories, we can either use the polynomial fitting method proposed by [12] to extract $\bar{\mathbf{x}}_l$, or simply divide $\mathbf{x}_l$ into several segments by its macroscopic states so that each segment has relatively steady macroscopic characteristics.

The above decomposition, albeit simple, can facilitate the analysis of traffic oscillations. For example, vehicle trajectories can be plotted into oblique coordinates to remove nominal components and preserve oscillatory components, so that we can easily use frequency analysis tools to measure oscillation characteristics. In addition, car-following models can be calibrated in the oblique coordinates by fitting the oscillatory components only.

2.2. Car-following model

Let v_* and v^* respectively denote the minimum and maximum possible vehicle speeds.[4] In our oscillation analysis, we are only interested in the non-trivial case where $v_* < \bar{v} < v^*$, because $\bar{v} = v_*$ or $\bar{v} = v^*$ implies that $\{\mathbf{x}_l\}_{\forall l}$ are a set of parallel straight lines without any oscillations. Recall that $\bar{v}$ and s_l reflect macroscopic traffic characteristics in stationary traffic (i.e., when $\hat{\mathbf{x}}_l = \{0\}_{t\in\mathbb{R}}$); for each l, we assume that they follow a velocity function $F_l : \mathbb{R} \to [v_*, v^*]$, such that $\bar{v} = F_l(s_l)$ (which can also be interpreted by a flow-density fundamental diagram from a macroscopic perspective). Here, we allow different vehicles to have different velocity functions so as to accommodate heterogeneous driving behavior.[5] When traffic is not stationary (i.e., when $\hat{\mathbf{x}}_l \neq \{0\}_{t\in\mathbb{R}}$), $F_l(s_l)$ may slightly deviate from $\bar{v}$.

We consider a class of car-following laws in the following form:

$$\left\{\frac{dx_l(t)}{dt}\right\}_{t\in\mathbb{R}} = \mathbf{G}_l[\{F_l(x_{l-1}(t) - x_l(t))\}_{t\in\mathbb{R}}], \forall l = 1, \cdots, L \tag{2}$$

where function $F_l(x_{l-1}(t) - x_l(t))$ is a target speed (based on the actual spacing) and $\mathbf{G}_l$ is an arbitrary linear operator (which might include differential, integral and time shift operations). In our analysis, we assume that F_l satisfies the following properties.

(i) $F_l(s)$ increases over $s \in \mathbb{R}$.

(ii) $F_l(s)$ is Lipschitz continuous; i.e., there exists a scalar $K_l \in \mathbb{R}_+$ such that $|F_l(s_1) - F_l(s_2)| \leq K_l|s_1 - s_2|, \forall s_1, s_2 \in \mathbb{R}$.

(iii) $F_l(s)$ is differentiable and strictly increasing when $F_l(s)$ is in the open set (v_*, v^*), and for all $v \in (v_*, v^*)$ there exists one and only one s such that $F_l(s) = v$ (or $s = F_l^{-1}(v)$). We define $\underline{s} = \lim_{v\to v_*^+} F_l^{-1}(v)$ and $\overline{s} = \lim_{v\to v^{*-}} F_l^{-1}(v)$.

Property (i) ensures that in congested traffic a lower vehicle density generally corresponds to a higher nominal speed. Property (ii) is satisfied by all continuous fundamental diagrams. Property (iii) reflects on the fact that during congestion a vehicle's speed is normally sensitive to its spacing changes. Many well-known continuous fundamental diagrams satisfy these three properties. For example, the Greenshield's fundamental diagram [50] can be specified by letting $F_l(s) = \max(v^* - v^* s_l^0/s, 0)$ where s_l^0 is the stopping distance and the Lipschitz scalar $K_l = v^*/s_l^0$. The triangle fundamental diagram [51, 52] can be specified by letting $F_l(s) = \left\lfloor \lambda_l(s - s_l^0) \right\rfloor_0^{v^*}$ where λ_l is a sensitivity coefficient, $\lfloor\cdot\rfloor_a^b := \mathrm{mid}(a, b, \cdot)$ and the Lipschitz scalar K_l is equal to λ_l.

We further assume that $\mathbf{G}_l$ satisfies the following two properties

(iv) The integral $\int \mathbf{G}_l$ is a low-pass filter; i.e., among all frequency components in its input time series, $\int \mathbf{G}_l$ amplifies low-frequency components more than high-frequency components.

(v) For any constant c, $\mathbf{G}_l(\{c\}_{t\in\mathbb{R}}) = \{c\}_{t\in\mathbb{R}}$.

Since an integral operation itself is a low-pass filter, property (iv) can be easily satisfied if $\mathbf{G}_l$ is not dominated by a differential operation. This is the case for most existing car-following laws. Property (v) explains the system's nominal behavior; i.e., it ensures that the macroscopic characteristics of the trajectories generated from (2) are consistent with those predicted by the fundamental diagram F_l.

[4] The minimum speed v_* is usually equal to 0 in the real world, but in our framework it may take any value.

[5] Actually, function F_l can be further generalized into a backlash nonlinear system [47] that contains two speed-spacing functions, one for deceleration and the other for acceleration. For the illustration of the proposed framework, this paper only focuses on the simple function form of F_l.

Plugging (1) into (2) yields

$$\left\{\frac{d\hat{x}_l(t)}{dt}\right\}_{t\in\mathbb{R}} = \mathbf{G}_l\left[\{F_l(\hat{x}_{l-1}(t) - \hat{x}_l(t) + s_l) - \bar{v}\}_{t\in\mathbb{R}}\right], \forall l = 1, \cdots, L \tag{3}$$

If we define a new function $\hat{F}_l(s) := F_l[s + F_l^{-1}(\bar{v})] - \bar{v}$ (note that $\hat{F}_l(0) = 0$), then (3) can be normalized as follows:

$$\left\{\frac{d\hat{x}_l(t)}{dt}\right\}_{t\in\mathbb{R}} = \mathbf{G}_l\left[\{\hat{F}_l(\hat{x}_{l-1}(t) - \hat{x}_l(t) + \bar{s}_l)\}_{t\in\mathbb{R}}\right], \forall l = 1, \cdots, L. \tag{4}$$

Here, $\bar{s}_l = s_l - F_l^{-1}(\bar{v})$ is an unknown variable that denotes the deviation of the actual spacing from what the fundamental diagram would predict. Before calculating the value of $\bar{s}_l$, we first introduce the following proposition.

Proposition 1. *Suppose F is continuous, increasing over $(-\infty, +\infty)$ and strictly increasing over (a, c) for some given $a < c \in \mathbb{R}$, and $\mathbf{y} = \{y(t)\}_{t\in\mathbb{R}}$ is an oscillatory series. Then for any $b \in (a, c)$, there exists one and only one scalar s such that $\{F(y(t) + s) - F(b)\}_{t\in\mathbb{R}}$ is an oscillatory series.*

Proof. See Appendix A □

If $a < 0 < c$, $F(0) = 0$, and $\mathbf{y}$ is an oscillatory time series, then we define a mapping $s := \bar{S}(\mathbf{y}, F)$ such that $\{F(y(t) + s)\}_{t\in\mathbb{R}}$ is a nominal time series. For some special $\mathbf{y}$ and F, we can compute $\bar{S}(\mathbf{y}, F)$ analytically. For example, if F is an odd function and $\mathbf{y}$ is a pure sinusoid, then $\bar{S}(\mathbf{y}, F) = 0$. In general, however, there might not exist an analytical method to compute $\bar{S}(\mathbf{y}, F)$. Rather, based on the monotonicity of F, we can obtain $\bar{S}(\mathbf{y}, F)$ from an efficient bisecting search method, as follows

Step C0: Initialize $s = 0$, and return s if $\int_0^P [F(y(t) + s)]dt = 0$; otherwise, let $s_- = a$ and $s_+ = 0$ if $\int_0^P [F(y(t) + s)]dt > 0$, or let $s_- = 0$ and $s_+ = c$ otherwise. Specify a small positive error tolerance ϵ.

Step C1: Let $s := (s_+ + s_-)/2$. If $|s_+ - s_-| < \epsilon$, return s; otherwise, go to Step C2.

Step C2: Let $s_- = s$ if $\int_0^P [F(y(t) + s')]dt < 0$, or let $s_+ = s$ otherwise. Go to Step C1.

Now we discuss how to solve $\bar{s}_l$. According to (4), since $\hat{\mathbf{x}}_l$ is an oscillatory series, so is $\left\{\frac{d\hat{x}_l(t)}{dt}\right\}_{t\in\mathbb{R}}$. Property (v) of $\mathbf{G}_l$ dictates that $\{\hat{F}_l(\hat{x}_{l-1}(t) - \hat{x}_l(t) + \bar{s}_l)\}_{t\in\mathbb{R}}$ shall also be purely oscillatory. We know that $\hat{\mathbf{x}}_{l-1} - \hat{\mathbf{x}}_l$ is an oscillatory series, function $\hat{F}$ is continuously increasing over $(-\infty, +\infty)$ and strictly increasing over $\left(\underline{s} - F_l^{-1}(\bar{v}), \overline{s} - F_l^{-1}(\bar{v})\right)$, $\underline{s} < F_l^{-1}(\bar{v}) < \overline{s}$, and $\hat{F}_l^{-1}(0) = 0$. Hence, for any given $\hat{\mathbf{x}}_{l-1} - \hat{\mathbf{x}}_l$ and $\hat{F}_l$, Proposition 1 indicates that $\bar{s}_l = \bar{S}(\hat{\mathbf{x}}_{l-1} - \hat{\mathbf{x}}_l, \hat{F}_l)$ can be obtained by Algorithm C0-C2. Then formula (4) can be equivalently expressed in terms of the oscillatory series only, as follows:

$$\hat{\mathbf{x}}_l = \int \mathbf{G}_l\left[\left\{\hat{F}_l\left(\hat{x}_{l-1}(t) - \hat{x}_l(t) + \bar{S}(\hat{\mathbf{x}}_{l-1} - \hat{\mathbf{x}}_l, \hat{F}_l)\right)\right\}_{t\in\mathbb{R}}\right] dt, \forall l = 1, \cdots, L. \tag{5}$$

Equation (5) can be used to express several well-known car-following models. The linear models [53, 22, 23] can be obtained by letting $v_* \to -\infty, v^* \to +\infty$ and F_l be an identity function. The fundamental diagram based models [54, 55, 56] and the OV models [26, 27] are also special cases of (5), with $\mathbf{G}_l$ being an identity mapping and an integral operation, respectively (see Section 4 for more detailed discussion).

3. Oscillation Characteristics Analysis

This section proposes a mathematical framework that analyzes stability properties and oscillation propagation characteristics for a class of nonlinear car-following laws (5). Stability analyses, including local and asymptotic stabilities, qualitatively explain whether a car following law will amplify or dampen a small trajectory perturbation over time and space. Local stability pertains to whether a perturbation at present will induce future fluctuations on the same trajectory [23]. Asymptotic stability concerns whether perturbations in the leading trajectory will amplify

across the following trajectories [22]. These traditional stability analysis methodologies are essentially the same for both linear and nonlinear car-following models, except that nonlinear models are usually linearized before these analyses.

If a car following law is both locally and asymptotically stable, it will dampen any perturbations from the leading vehicle and therefore all following vehicles will always move smoothly. This, however, is not consistent with empirical observations. Unstable models will amplify certain perturbations in the leading trajectory and certain oscillation patterns will propagate across trajectories. We will propose an analytical approach that quantitatively predicts the propagation of oscillation characteristics (e.g., periodicity and magnitude) in a vehicle platoon for an unstable nonlinear car-following law in the form of (2). This approach is built on the describing function method [47] from the nonlinear control literature, which is often used to quantify oscillation responses of a nonlinear system for a given sinusoidal input. With this method as a building block, the proposed approach is able to handle the nonlinearity in (2) from a frequency domain perspective and yield an accurate analytical prediction of traffic oscillation propagation.

3.1. Stability analysis

This section introduces methods to analyze the local and asymptotic stability properties of car-following law (5). The local stability pertains to whether the following vehicle's trajectory can stabilize to its nominal state over time, despite a small perturbation from its immediate preceding vehicle [23]. The asymptotic stability describes whether perturbations from the leading vehicle's trajectory will be amplified across vehicles upstream [22]. It shall be noted that asymptotic stability is only well defined for car-following laws that are locally stable. For the convenience of the notation, we denote the value of $\mathbf{G}_l(\cdot)$ at t by $G_l(\cdot, t)$, i.e., $\mathbf{G}_l(\cdot) = \{G_l(\cdot, t)\}_{t\in\mathbb{R}}$. Local stability analysis is generally based on the linearization of car-following law (5). Define the Laplace transform of the linear operation $\mathbf{G}_l$

$$\mathcal{G}_l^L(r) := \lim_{T\to\infty} \frac{\int_0^T G_l(\{e^{-rt}\}, t)dt}{\int_0^T e^{-rt}dt}, \forall r \in \mathbb{C}, \tag{6}$$

then the linearized characteristic equation of (5) in the Laplace space is defined as

$$\frac{\mathcal{G}_l^L(r)}{r} \left.\frac{d\hat{F}_l(s)}{ds}\right|_{s=0} + 1 = 0, \forall r \in \mathbb{C}, \tag{7}$$

Equation (7) is the denominator of the close-loop transfer function for (5) (see [57] for the introduction to a close-loop system). Car-following law (5) is locally stable if every solution r to (7) (which is a pole of the close-loop transfer function) is within the left half complex plane; i.e., the real part of the solution is negative.

For a locally stable car-following law, asymptotic stability can be analyzed based on the frequency response gain of the linearized car-following law (5). Define a complex function

$$\mathcal{G}_l(\omega) := \mathcal{G}_l^L(j\omega) = \frac{j}{\pi}\int_{-\pi}^{\pi} G_l(\{e^{-\omega t}\}, t)e^{-j\omega t}d\omega t, \forall w \in \mathbb{R}_+. \tag{8}$$

where $j = \sqrt{-1}$ and $G_l(\omega, t)$ is the value of $\mathbf{G}_l(\{\sin(\omega t)\}_{t\in\mathbb{R}})$ at time t. Function (8) is the Fourier transform [58] of the linear system $\mathbf{G}_l$, which is also called the frequency transfer function. The measure for asymptotic stability can be defined as follows

$$\left| \frac{\mathcal{G}_l(j\omega) \left.\frac{d\hat{F}_l(s)}{ds}\right|_{s=0}}{\mathcal{G}_l(j\omega) \left.\frac{d\hat{F}_l(s)}{ds}\right|_{s=0} + j\omega} \right|, \forall \omega \in \mathbb{R}_+. \tag{9}$$

Car-following law (5) is asymptotically stable if the value of (9) is uniformly no larger than 1 for all $\omega \in \mathbb{R}_+$.

3.2. Oscillation characteristic quantification

3.2.1. Limit cycle analysis for locally unstable car-following laws

For a locally unstable nonlinear car-following law (5), if the value of function F_l is bounded, a leading vehicle's perturbation shall just lead to bounded oscillation (or a limit cycle [47]) in the following vehicles' trajectories

(rather than increasing toward infinity). In this section we will show how to calculate the oscillation propagation characteristics for nonlinear car-following law (5).

Let $\hat{x}_{l-1}(t) = 0, \forall t$, and then (5) becomes

$$\hat{\mathbf{x}}_l = \int \mathbf{G}_l \left[\left\{ \hat{F}_l(-\hat{x}_l(t) + \bar{s}_l) \right\}_{t\in\mathbb{R}} \right] dt, \forall l = 1, \cdots, L \tag{10}$$

Assume time series $\hat{\mathbf{x}}_l$ can be approximated by a sinusoid $\{A_l \sin(\omega t + \phi_l)\}_{t\in\mathbb{R}}$ with amplitude $A_l \in \mathbb{R}_+$, frequency $\omega \in \mathbb{R}_+$ and phase angle $\phi_l \in [0, 2\pi)$. Hence $\{\hat{F}_l(-\hat{x}_l(t) + \bar{s}_l)\}_{t\in\mathbb{R}}$ shall also include frequency ω, but due to nonlinearity, it may contain sinusoidal components of higher frequencies. Fortunately, these higher frequencies, if any, will likely be dampened by the low-pass filter $\int \mathbf{G}_l$. Thus, the describing function method [47] just considers the fundamental sinusoidal component of $\{\hat{F}_l(-\hat{x}_l(t)+\bar{s}_l)\}_{t\in\mathbb{R}}$. Then, it can be derived that equation (10) can be approximately represented in the frequency domain as follows,

$$\mathcal{F}_l(A_l) - \frac{-j\omega}{\mathcal{G}_l(\omega)} \approx 0, \tag{11}$$

where

$$\mathcal{F}_l(A) := \frac{\int_{-\pi}^{\pi} \left[\hat{F}_l \left(A \sin(t) + \bar{S}\left(\{A \sin(t)\}_{t\in\mathbb{R}}, \hat{F}_l \right) \right) \right] e^{-jt} dt}{\int_{-\pi}^{\pi} A \sin(t) e^{-jt} dt} \tag{12}$$

$$= \int_{-\pi}^{\pi} \left[\hat{F}_l \left(A \sin(t) + \bar{S}\left(\{A \sin(t)\}_{t\in\mathbb{R}}, \hat{F}_l \right) \right] e^{-j(t-\pi/2)} dt, \forall A \neq 0 \in \mathbb{C} \tag{13}$$

See Appendix B for the detailed derivation of (11).

Solving this complex-valued equation (11) (which is equivalent to two real-valued equations) yields the candidate frequency ω and amplitude A_l for the limit cycle in $\hat{\mathbf{x}}_l$. In cases (11) cannot be solved analytically, we can solve it numerically in the following way. Note that $\{\mathcal{F}_l(A_l)\}_{A_l\in\mathbb{R}}$ and $\{-j\omega/\mathcal{G}_l(\omega)\}_{\omega\in\mathbb{R}}$ are two curves on the complex plane. Since $|\mathcal{F}_l(\cdot)| \in [0, K_l]$, $\{\mathcal{F}_l(A_l)\}_{A_l\in\mathbb{R}}$ shall lie within a circle which has radius K_l and is centered at the origin. If $\{-j\omega/\mathcal{G}_l(\omega)\}_{\omega\in\mathbb{R}}$ lies outside this circle, there is no solution to (11) and the car-following law should be locally stable. Otherwise, we just need to find the intersection(s) of these two curves. For a given ω, it is easy to evaluate the transfer function $\mathcal{G}_l(\omega)$. For a given A_l, it is also easy to evaluate $\mathcal{F}_l(A_l)$ (from Algorithm C0-C2) to obtain $\bar{S}(\{A_l \sin(t)\}_{t\in\mathbb{R}}, \hat{F}_l)$ and then calculating (12). Hence, we can find the intersection(s) by enumerating a reasonable range of A_l and ω values.[6] After obtaining such an intersection, we need to verify its stability; i.e., stable solution (ω, A_l) shall satisfy $|\mathcal{F}_l(A_{l-})| > |\frac{-j\omega}{\mathcal{G}_l(\omega)}|$ for an A_{l-} slightly smaller than A_l and $|\mathcal{F}_l(A_{l+})| < |\frac{-j\omega}{\mathcal{G}_l(\omega)}|$ for an A_{l+} slightly greater than A_l. Only the stable solution(s) is suitable for quantification of the oscillation characteristics for the limit cycle.

3.2.2. Oscillation propagation analysis for locally stable car-following laws

However, many car-following models capable of reproducing traffic oscillations are locally stable but asymptotically unstable. For such car-following laws, we will propose a describing-function-based method to quantify oscillation characteristics for each generated trajectory. These oscillation characteristics quantitatively predict how small perturbations of vehicle 0 are amplified into fully-grown oscillations across the following vehicles $l = 1, 2, \cdots, L$.

Suppose that $\hat{\mathbf{x}}_0$ can be approximated by a single sinusoid of frequency ω. In car-following law (5), suppose that the input $\hat{\mathbf{x}}_{l-1}$ can be approximated by a sinusoid $\{A_{l-1} \sin(\omega t)\}_{t\in\mathbb{R}}$ where A_{l-1} is the amplitude.[7] Since $\hat{\mathbf{x}}_l$ is generated from $\hat{\mathbf{x}}_{l-1}$, it shall also preserve the same periodicity. The low-pass property of $\int \mathbf{G}_l$ says that $\hat{\mathbf{x}}_l$ shall also follow a sinusoidal shape (although the phase angle might have changed). This means that all $\hat{\mathbf{x}}_l, \forall l = 1, 2, \cdots, L$, can be approximated by sinusoids of the same frequency ω. Suppose $\hat{x}_l(t)$ is approximated with $A_l \sin(\omega t + \phi_l)$ where A_l and ϕ_l are, respectively, the amplitude and the phase angle of $\hat{\mathbf{x}}_l$. Then (5) can be represented as

$$\{A_l \sin(\omega t + \phi_l)\}_{t\in\mathbb{R}} \approx \int \mathbf{G}_l \left[\left\{ |\vec{A_l}| \mathcal{F}_l(|\vec{A_l}|) | \sin\left[\omega t + \angle(\vec{A_l}) + \angle(\mathcal{F}_l(|\vec{A_l}|)) \right] \right\}_{t\in\mathbb{R}} \right] dt. \tag{14}$$

[6] For most car-following laws in the literature, there is usually no more than one intersection.

[7] This expression does not include a phase angle because we can always shift the time axis to remove it.

where $\vec{A_l} = A_{l-1} - A_l e^{j\phi_l}$. The frequency domain representation of (14) is

$$A_l e^{j\phi_l} \approx \frac{\mathcal{G}_l(\omega)}{j\omega}\mathcal{F}_l(|\vec{A_l}|)\vec{A_l}. \tag{15}$$

or

$$A_l e^{j\phi_l}\left(1 + \frac{\mathcal{G}_l(\omega)}{j\omega}\mathcal{F}_l(|\vec{A_l}|)\right) \approx \frac{\mathcal{G}_l(\omega)}{j\omega}\mathcal{F}_l(|\vec{A_l}|)A_{l-1}. \tag{16}$$

If the oscillatory component of $\hat{\mathbf{x}}_{l-1}$ is given as $x_l(t) = A\sin(\omega t)$, the oscillation characteristics A_l and ϕ_l for $\hat{\mathbf{x}}_l$ can be quantified using Equation (16). If the analytical solution is difficult to obtain, it can be solved numerically as follows:

Step A0: Initialization. Let $\mathcal{F}^0 = K_l, k = 0$.

Step A1: Let

$$A_l^k = \frac{\mathcal{G}_l(\omega)\mathcal{F}^k}{j\omega + \mathcal{G}_l(\omega)\mathcal{F}^k}A_{l-1}.$$

Step A2: Let $\mathcal{F}^{k+1} = \beta\mathcal{F}_l(|A_{l-1} - A_l^k|) + (1-\beta)\mathcal{F}^k$ with a proper scalar $\beta \in (0,1)$.

Step A3: Stop if $\{A_l^k\}$ converges, and output $A_l = |A_l^{k+1}|$ and $\phi_l = \angle(A_l^{k+1})$; otherwise, $k = k+1$ and go to Step A1.

For any given ω and A_{l-1}, the above approach can be used to obtain A_l. Define the amplitude amplification ratio $R(A_{l-1}, \omega) := A_l/A_{l-1}$. We can create a surface for the amplification ratio $\{R(A_{l-1},\omega)\}_{A_{l-1},\omega\in\mathbb{R}_+}$ for all possible ω and A_{l-1} values. If F_l is linear, the surface will no longer depend on A_l and shall degrade to a single curve (i.e., the Bode plot), which is exactly the frequency response (9). So we call this surface the generalized frequency response, which can be used to quantify oscillation propagation for a given leading trajectory $\hat{\mathbf{x}}_0$.

For a linear car-following model, propagation (and amplification) of each frequency component is independent, and hence $\hat{\mathbf{x}}_0$ can be decomposed into a set of individual sinusoids and the propagation of each sinusoid can be independently quantified. As such, $\hat{\mathbf{x}}_l$ can be obtained by superposition of all these sinusoids. However, for a nonlinear model in the form of (5), different frequency components may significantly interfere with each other during propagation. The propagation and growth of traffic oscillations can be quantified as follows.

In case $\hat{\mathbf{x}}_0$ is a pure sinusoid, i.e., $\hat{x}_0(t) = A_0\sin(\omega t)$, with a fixed frequency $\omega \in \mathbb{R}_+$ and a very small amplitude $A_0 \in \mathbb{R}_+$, we can look up the corresponding amplification ratio at frequency ω in the generalized frequency response surface and calculate the oscillation amplitude of the next vehicle trajectory. This can be repeated for all L vehicles to obtain values for $A_1, \cdots, A_L$. We can also repeat this for all $\omega \in \mathbb{R}_+$, and we obtain an oscillation propagation surface $\{A_l\}_{\omega\in\mathbb{R}_+, l=0,\cdots,L}$.

In real data, $\hat{\mathbf{x}}_0$ is likely to include random perturbations rather than a pure sinusoid [12]. Since function $\hat{F}_l$ is differentiable around the origin, we can first treat the car-following law as a linear law when the oscillation magnitude is small (e.g., for the first few downstream vehicles), and we use the above described decomposition-superposition approach to quantify the oscillation propagation. As a result, the frequency components that result in highest values on the generalized frequency response surface for small A_{l-1} will be amplified the most. We call these frequency components "dominating." Once the oscillation magnitude grows larger so that the nonlinear effect of the car-following law is significant, we will approximate $\hat{\mathbf{x}}_l$ with a pure sinusoid (which shall be of one of the previous dominating frequencies) and only analyze this frequency component for all the following trajectories.

4. Numerical Examples

The modeling framework proposed in Section 3 can obviously be applied to a wide range of car-following laws (i.e., with different fundamental diagram function F_l and operator $\mathbf{G}_l$). For illustration purposes, we will consider a few well-known examples and compare the analytical oscillation propagation predictions with those observed in numerical simulations.

4.1. Examples of F_l and $\mathbf{G}_l$

We will consider the following two types of F_l.

Newell's Model. We first consider the case where function F_l is the velocity-spacing representation of a triangular flow-density fundamental diagram [59]; see Figure 2.[8] Parameters v^* and s_l^0 are the free-flow speed (or the posted speed limit) and the stopping distance, respectively. Scalar λ_l is a sensitivity factor that reflects the aggressiveness of the driver [61]. The mathematical expression for F_l is

$$F_l(s) = \left\lfloor \lambda_l (s - s_l^0) \right\rfloor_0^{v^*} \tag{17}$$

Note that expression (17) satisfies Properties (i)-(iii) with $v_* = 0$ and $K_l = \lambda_l$. It is easy to show that

$$\hat{F}_l(s) = \lfloor \lambda_l s \rfloor_{-\bar{v}}^{v^*-\bar{v}}. \tag{18}$$

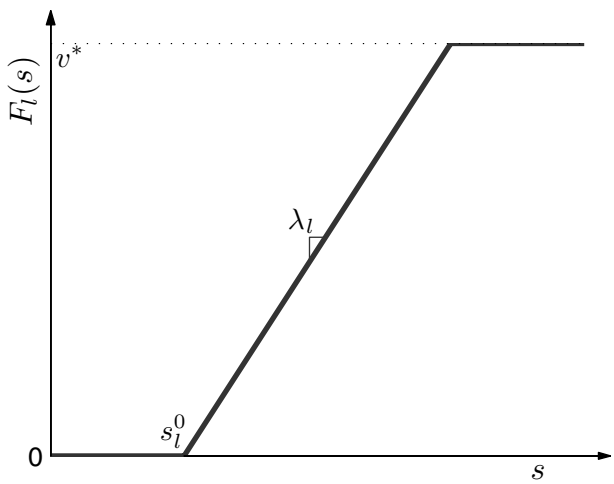

Figure 2: Triangular fundamental diagram based F_l.

Then complex function $\mathcal{F}_l$ can be derived as follows,

$$\mathcal{F}_l(A) := \frac{2}{A\pi}\left[\frac{A\lambda_l}{4}\left(e^{-j(2\phi+\pi/2)} - e^{-j(2\sigma+\pi/2)}\right) + (v^* - \bar{v} - \lambda_l \bar{s}_l)e^{-j\phi} + (\bar{v} + \lambda_l \bar{s}_l)e^{-j\sigma} + (v^* - 2\bar{v})e^{j\pi/2} + \frac{\lambda_l}{2}(\phi - \sigma)\right], \forall A \in \mathbb{R}_+, \tag{19}$$

where

$$\sigma = \begin{cases} \sin^{-1}\left(\frac{-\bar{s}_l - \bar{v}/\lambda_l}{A}\right) & \text{if } -A < \bar{s}_l < A - \bar{v}/\lambda_l; \\ -\pi/2 & \text{if } A - \bar{v}/\lambda_l \le \bar{s}_l < A. \end{cases},$$

$$\phi = \begin{cases} \sin^{-1}\left(\frac{-\bar{s}_l + (v^* - \bar{v})/\lambda_l}{A}\right) & \text{if } -A + (v^* - \bar{v})/\lambda_l < \bar{s}_l < A; \\ \pi/2 & \text{if } -A < \bar{s}_l \le -A + (v^* - \bar{v})/\lambda_l \end{cases}$$

[8] A triangular fundamental diagram is simple yet capable of explaining the constant backward wave speed observed in reality [60]. Note that it is not differentiable everywhere.

and $\bar{s}_l = \bar{S}(\{A\sin(t)\}_{t\in\mathbb{R}}, \hat{F}_l)$ can be obtained by solving the following equation via Algorithm C0-C2,

$$\int_{-\pi/2}^{\pi/2}[\hat{F}(A\sin(t)+\bar{s}_l)]dt = -\bar{v}\left(\sigma+\frac{\pi}{2}\right)+(v^*-\bar{v})\left(\frac{\pi}{2}-\phi\right)+\bar{s}_l(\phi-\sigma)+A(\cos(\sigma)-\cos(\phi))=0. \tag{20}$$

Note that if $2\bar{v} = v^*$,

$$\mathcal{F}_l(A) = \frac{2\lambda_l}{\pi}\left[\sin^{-1}\left(\frac{v^*/\lambda_l}{2A}\right) + \frac{v^*/\lambda_l}{2A}\sqrt{1-\left(\frac{v^*/\lambda_l}{2A}\right)^2}\right].$$

and $\bar{S}(\{A\sin(t)\}_{t\in\mathbb{R}}, \hat{F}_l) = 0$.

OV Model. Another popular form of F_l can be drawn from the OV model [26, 27], as illustrated in Figure 3. Its function form can now be specified as follows

$$F_l(s) = \frac{v^*}{2}\left(\tanh(\frac{2\lambda_l(s-s_l^m)}{v^*})+1\right), \tag{21}$$

where s_l^m is a scalar and $\tanh(z) = (e^z - e^{-z})/(e^z + e^{-z}), \forall z \in \mathbb{R}$ is the hyperbolic tangent function. Equation (21) also satisfies Properties (i)-(iii) with $v_* = 0$ and $K_l = \lambda_l$. The shape of (21) is similar to that of (17), although the boundary conditions of (21) are somehow unrealistic (e.g., equation (21) does not yield a positive stopping distance and the target speed can never reach v^* for any s). However, the differentiability of this function are favorable for stability analysis [26].

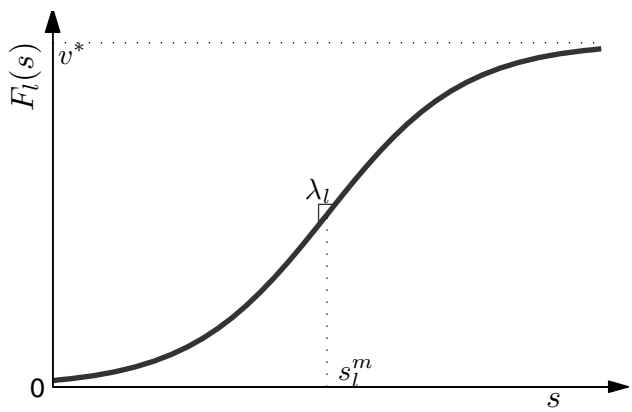

Figure 3: Hyperbolic tangent based F_l.

The corresponding $\hat{F}_l$ function can be shown to be

$$\hat{F}_l(s) = \frac{v^*}{2}\tanh\left(\frac{2\lambda_l s_l}{v^*}+\tanh^{-1}\left(\frac{2\bar{v}}{v^*}-1\right)\right)+\frac{v^*}{2}-\bar{v}. \tag{22}$$

In this case, $\mathcal{F}_l$ does not have an analytical expression in terms of ω, and hence we will numerically solve $\bar{s}_l = \bar{S}(\{A\sin t\}_{t\in\mathbb{R}}, \hat{F}_l)$ from the following equation via Algorithm C0-C2:

$$\int_{-\pi/2}^{\pi/2}\left[\frac{v^*}{2}\tanh\left(\frac{2\lambda_l A\sin(t)}{v^*}+\tanh^{-1}\left(\bar{v}-\frac{v^*}{2}\right)\right)+\frac{v^*}{2}-\bar{v}\right]dt = 0. \tag{23}$$

Benchmark: Linear Model. For comparison purposes, we define a benchmark linear function $F_l(s)$ as follows.

$$F_l(s) = \lambda_l(s-s_l^0), \tag{24}$$

which can be equivalently transformed into

$$\hat{F}_l(s) = \lambda_l s, \tag{25}$$

and

$$\mathcal{F}_l(A) = \lambda_l. \tag{26}$$

Note that the slopes of (18), (22) and (25) are all the same at the origin. This implies that these three car-following laws shall lead to similar oscillation propagation when oscillation magnitudes are very small.

We also consider the following two types of operator $\mathbf{G}_l$:

Speed Following. In some car following models [22, 23, 54], $\mathbf{G}_l$ is a simple time shift operator,

$$\mathbf{G}_l\{y(t)\}_{t\in\mathbb{R}} = \{y(t-\tau_l)\}_{t\in\mathbb{R}}, \tag{27}$$

where τ_l is the driver's time lag. This operator implies each vehicle l will exactly follow the target speed based on the spacing observed τ_l time ago. Equations (6) and (9) now become

$$\mathcal{G}_l^L(r) = e^{-r\tau_l}, \tag{28}$$

and

$$\mathcal{G}_l(\omega) = e^{-j\omega\tau_l}. \tag{29}$$

Speed Target. Operator $\mathbf{G}_l$ may also be drawn from the OV model such that the acceleration of a vehicle is proportional to the difference of its actual speed and the target speed observed τ_l time ago. That is, if the following vehicle's current speed $\{y'(t)\}_{t\in\mathbb{R}} = \mathbf{G}_l(\{y(t)\}_{t\in\mathbb{R}})$, then

$$\frac{dy'(t)}{dt} = \alpha(y(t-\tau_l) - y'(t-\tau_l)), \tag{30}$$

where α is a positive scalar. Equation (7) and (9) can be derived easily as follows

$$\mathcal{G}_l^L(r) = \frac{\alpha}{re^{r\tau_l} + \alpha}, \tag{31}$$

and

$$\mathcal{G}_l(\omega) = \frac{\alpha}{j\omega e^{j\omega\tau_l} + \alpha}. \tag{32}$$

In the following subsections we will analyze the four possible combinations of F_l and $\mathbf{G}_l$.[9] For each case, we will first examine the local and asymptotic stabilities, and then quantify oscillation propagation properties.

4.2. Case 1: Newell's F_l and Speed Following $\mathbf{G}_l$

From (18), we obtain the slope

$$\left.\frac{d\hat{F}_l(s)}{ds}\right|_{s=0} = \lambda_l.$$

To obtain the root(s) of (7), we need to solve

$$\frac{\lambda_l e^{-r\tau_l}}{r} + 1 = 0. \tag{33}$$

Obviously, for any root of (33), the real part is negative if and only if $\lambda_l\tau_l < \pi/2$. Hence, as well known in the literature [23], this car-following law is locally stable if the sensitivity scalar $\lambda_l < \pi/(2\tau_l)$.

With regard to asymptotic stability, (9) becomes

$$\left|\frac{\lambda_l}{j\omega e^{j\omega\tau_l} + \lambda_l}\right|. \tag{34}$$

[9] Note that (5) becomes the OV car-following model in [27] if OV F_l and Speed Target $\mathbf{G}_l$ are combined.

The maximum absolute value of (34) over $\omega \in \mathbb{R}_+$ is smaller than 1 if and only if $\lambda_l \tau_l < 0.5$. Hence, as shown in [22], this car-following law is asymptotically stable if $\lambda_l < 1/(2\tau_l)$.

It shall be noted that since (7) and (9) are based on a linearized car-following law, the stability results shall be the same for other forms of $\hat{F}_l(s)$ as long as the slope at $s = 0$ is preserved (e.g, (22) and (25)).

For a locally unstable car-following law, we can quantify its limit cycle characteristics with the method proposed in Section 3.1. Figure 4 shows the numerical results for different $\bar{v}$, λ_l and τ_l values. We see that for a given $\bar{v}$, the amplitude A increases with λ_l and τ_l. The oscillation period $2\pi/\omega$ is around $4\tau_l$ for all different settings (it is exactly $4\tau_l$ when $\bar{v} = 0.5v^*$). These results are consistent with simulation outcomes.

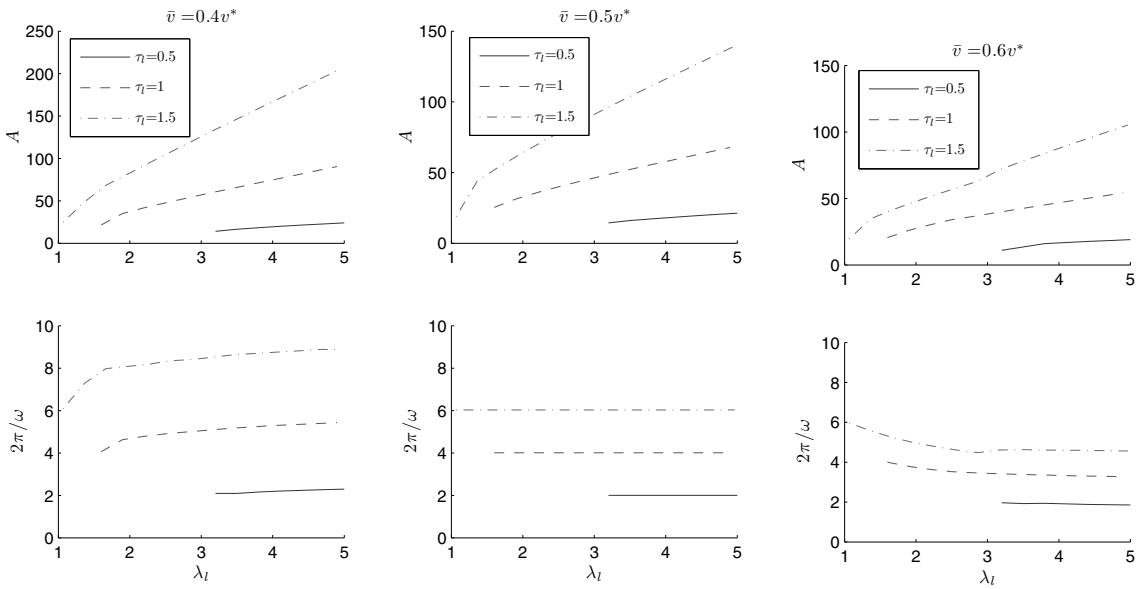

Figure 4: Limit cycle characteristics for Case 1 ($v^* = 50$).

We can also quantify the oscillation propagation in a vehicle platoon. For illustration purposes, we set $\tau_l = \lambda_l = 1$ and $v^* = 50$. Now $\tau_l = 1/\lambda_l$, which is consistent with the conjecture that the backward shock wave speed equals s_l^0/τ_l [61]. Since $0.5 < \lambda_l \tau = 1 < \pi/2$, the car-following law is locally stable but asymptotically unstable. Figure 5 plots amplification ratio $\{R(A_{l-1}, \omega)\}_{A_{l-1}, \omega \in \mathbb{R}_+}$ and oscillation magnitude $\{A_l\}_{\omega \in \mathbb{R}_+, l=0,\cdots,L}$ that are obtained from Algorithm A0-A3. We see that for a given frequency, the oscillation amplitude grows to a certain bound value and then flattens out, which is consistent with empirical observations [12].

The results in Figure 5 give us a way to predict oscillation propagation for any leading vehicle trajectory $\hat{\mathbf{x}}_0$; some examples are shown in Figure 6. We conduct the simulation with the car-following model for a certain given leading vehicle trajectory $\mathbf{x}_0$ (which is specified by $\hat{x}(t)$ and $\bar{v}$ in Figure 6), and we obtain a platoon of trajectories of the following vehicles. Then we decompose these trajectories into nominal and oscillatory components (see Figure 1), and plot the magnitudes of the oscillatory components from downstream to upstream as the blue solid curves in Figure 6. Then we apply the proposed analytical approach to predict the oscillation magnitudes with the same input $\mathbf{x}_0$, which are plotted as the green dashed curves. For comparison, we also plot the predictions from the corresponding linear model as red dot-dashed curves. Note that in Figure 6, the oscillation magnitude is measured by the standard deviation (STD) of $\hat{\mathbf{x}}_l$ (rather than A_l) to accommodate non-sinusoidal $\hat{\mathbf{x}}_l$. As we discussed in Section 3.2, when $\hat{\mathbf{x}}_0$ is a pure sinusoid, the frequency of $\hat{\mathbf{x}}_l, \forall l$ will remain the same; when $\hat{\mathbf{x}}_0$ is a random time series, we analyze the first 5 vehicles with the decomposition-superposition approach across all frequency components and then focus on the most dominating frequency component for the rest of following vehicles. We see that for different $\bar{v}$ values and input patterns, the predicted oscillation magnitudes generally are very close to those obtained in simulations; especially, they

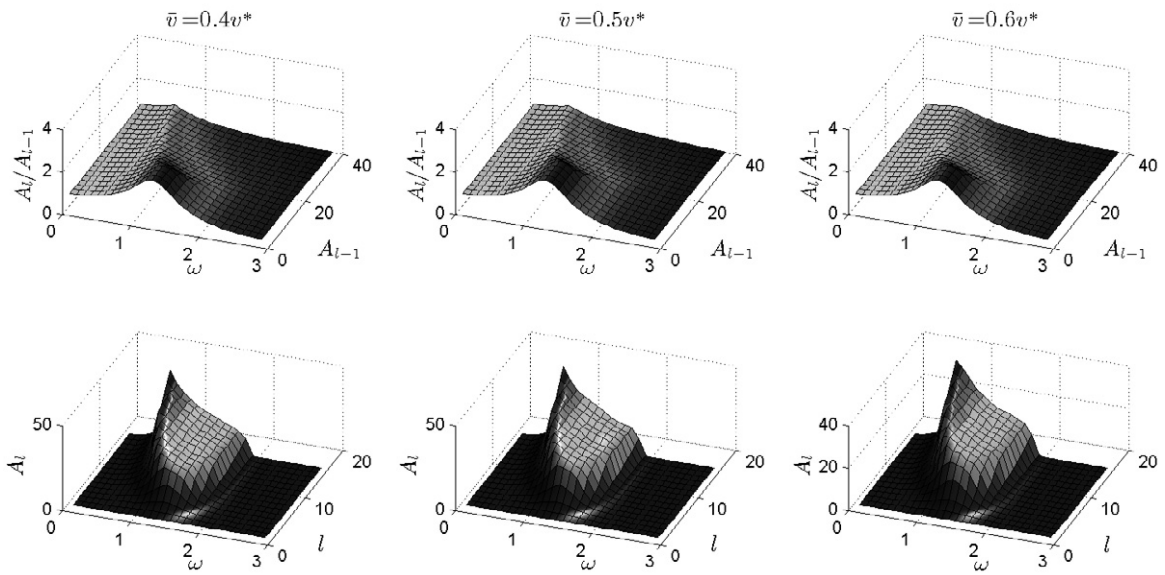

Figure 5: $\{R(A_{l-1},\omega)\}_{A_{l-1},\omega\in\mathbb{R}_+}$ and $\{A_l\}_{\omega\in\mathbb{R}_+,l=0,\cdots,L}$ surfaces for Case 1.

are almost overlapping when $\bar{v} = v^*/2$. Note how, in contrast, the linear model yields unbounded oscillation growth, while the proposed approach has successfully produced the growing-and-flattening pattern of oscillation propagation resulted from nonlinear car-following laws.

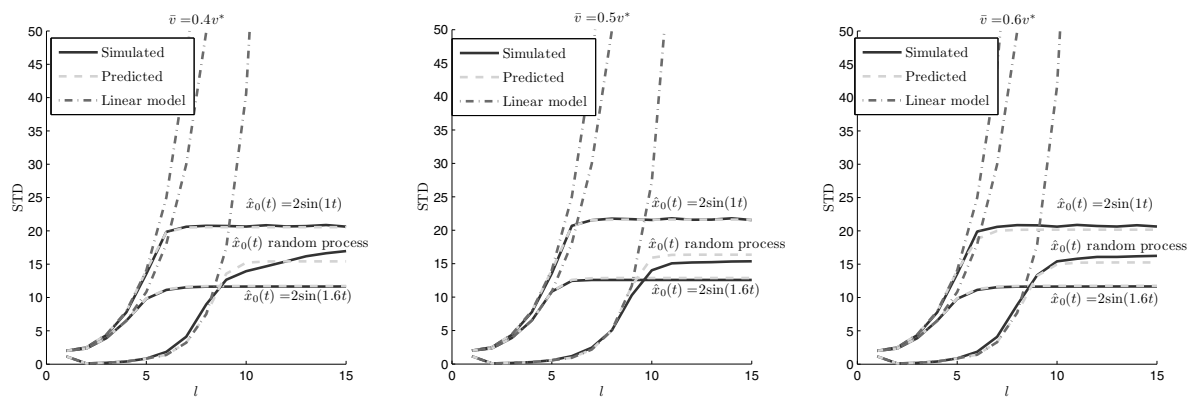

Figure 6: Prediction of oscillation propagation for Case 1.

4.3. Case 2: Newell's F_l and Speed Target $\mathbf{G}_l$

Equation (7) becomes

$$\frac{\lambda_l\alpha}{r^2e^{r\tau_l}+\alpha r}+1=0.$$

or

$$r^2e^{r\tau_l}+\alpha r+\lambda_l\alpha=0. \tag{35}$$

Equation (35) does not have closed-form analytical solutions and shall be solved numerically. For illustration purposes, we set $\tau_l = 0$.[10] The solution to (35) is

$$r = -\frac{\alpha}{2} \pm \frac{\sqrt{\alpha^2 - 4\alpha\lambda_l}}{2},$$

which always has a negative real part. This implies this car-following model is always locally stable when $\tau_l = 0$.

Regarding asymptotic stability, Equation (9) becomes

$$\left| \frac{-\omega^2 e^{j\omega\tau_l} + j\alpha\omega}{\lambda_l \alpha} + 1 \right|^{-1}. \tag{36}$$

The maximum value of (36) has to be numerically solved too. When $\tau_l = 0$, the maximum value of (36) over $\omega \in \mathbb{R}_+$ is greater than 1 if $\alpha < 2\lambda_l$ (which is consistent with the results from [26]).

We now quantify the oscillation propagation when $\tau_l = 0$, $\alpha_l = 1$, $\lambda_l = 1$ and $v^* = 50$. The car-following law under these parameters is also locally stable but asymptotically unstable. Figure 7 shows the amplification ratio $\{R(A_{l-1}, \omega)\}_{A_{l-1},\omega\in\mathbb{R}_+}$ and oscillation propagation $\{A_l\}_{\omega\in\mathbb{R}_+,l=0,\cdots,L}$. The dominating frequencies in Figure 7 are generally

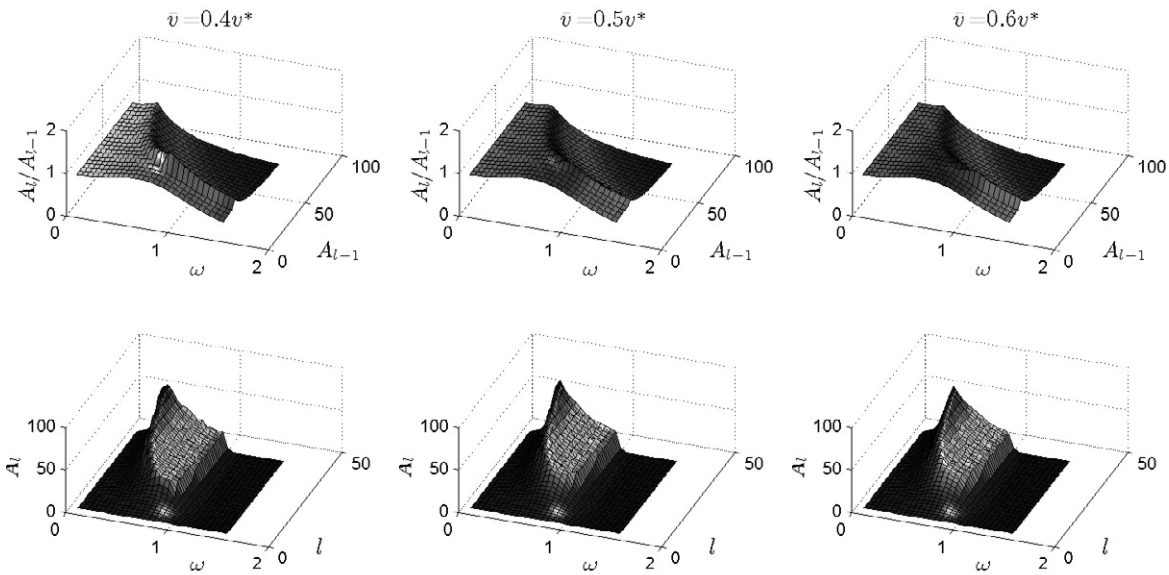

Figure 7: $\{R(A_{l-1}, \omega)\}_{A_{l-1},\omega\in\mathbb{R}_+}$ and $\{A_l\}_{\omega\in\mathbb{R}_+,l=0,\cdots,L}$ surfaces for Case 2.

smaller than those in Figure 5, which implies that Speed Target $\mathbf{G}_l$ tends to generate a larger oscillation period. Figure 8 plots the predicted oscillation magnitudes for different $\bar{v}$ and $\hat{\mathbf{x}}_0$. Again, we see the predicted and simulated results match each other and converge to a finite bound.

4.4. Case 3: OV's F_l and Speed Following $\mathbf{G}_l$

Since OV's F_l has the same slope λ_l at the origin as that in Case 1, the stability analysis results shall be the same as well. Again, we set $\tau_l = 1$, $\lambda_l = 1$ and $v^* = 50$. Figure 9 plots $\{R(A_{l-1}, \omega)\}_{A_{l-1},\omega\in\mathbb{R}_+}$ and $\{A_l\}_{\omega\in\mathbb{R}_+,l=0,\cdots,L}$. All surfaces in Figure 9 are smoother than those in Figure 5 because OV's F_l is smoother than Newell's F_l. Figure 10 predicts

[10] Zero time lag has also been assumed in other oscillation analysis such as [26].

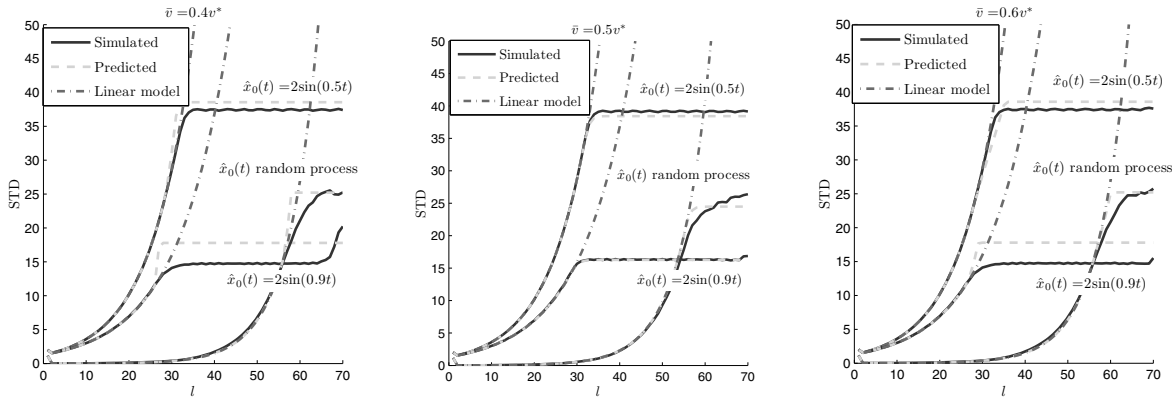

Figure 8: Prediction of oscillation propagation for Case 2.

oscillation propagation for different $\bar{v}$ and $\hat{\mathbf{x}}_0$, which are consistent with simulation results. The magnitude growth also seems smoother.

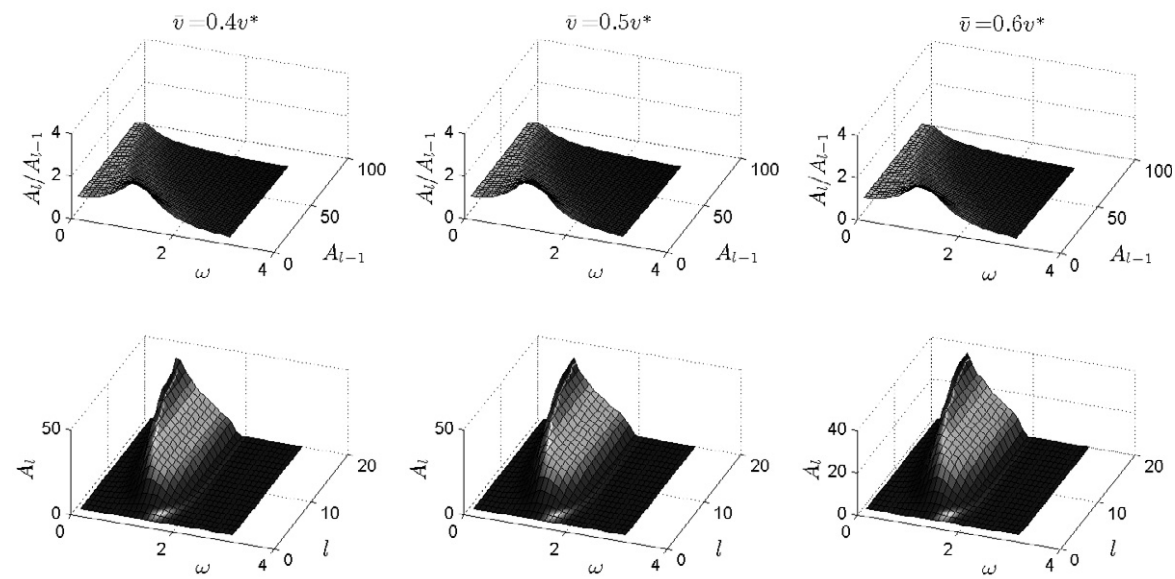

Figure 9: $\{R(A_{l-1},\omega)\}_{A_{l-1},\omega\in\mathbb{R}_+}$ and $\{A_l\}_{\omega\in\mathbb{R}_+,l=0,\cdots,L}$ surfaces for Case 3.

4.5. Case 4: OV's F_l and Speed Target $\mathbf{G}_l$

The car-following law in this case is exactly the OV model [26, 27], and the stability results shall be the same as those in Case 2. While the parameters are the same as those in Case 2 (i.e., $\tau_l = 0$, $\alpha_l = 1$, $\lambda_l = 1$ and $v^* = 50$), the $\{R(A_{l-1},\omega)\}_{A_{l-1},\omega\in\mathbb{R}_+}$ and $\{A_l\}_{\omega\in\mathbb{R}_+,l=0,\cdots,L}$ surfaces in Figure 11 are smoother than the counterparts in Figure 7. The oscillation magnitude growth predictions in Figure 12 are again consistent with simulation results, and they also seem smoother than those in Case 2.

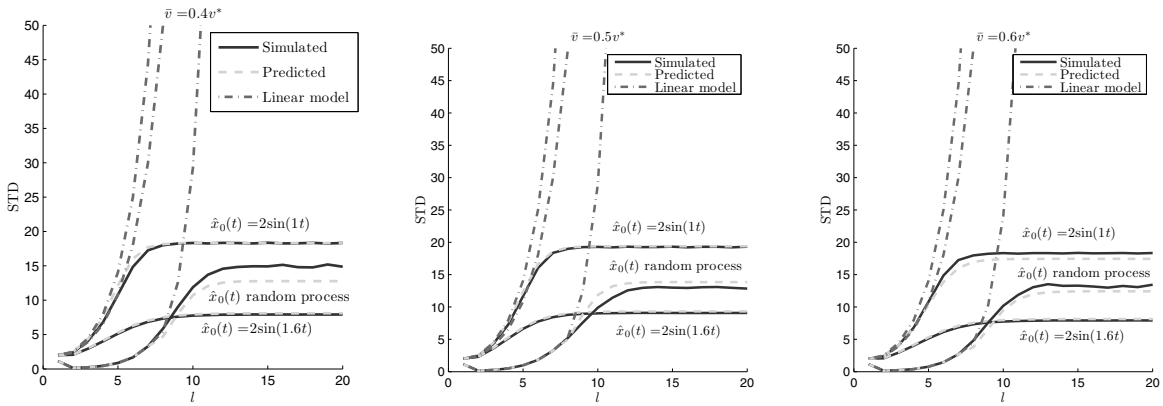

Figure 10: Prediction of oscillation propagation for Case 3.

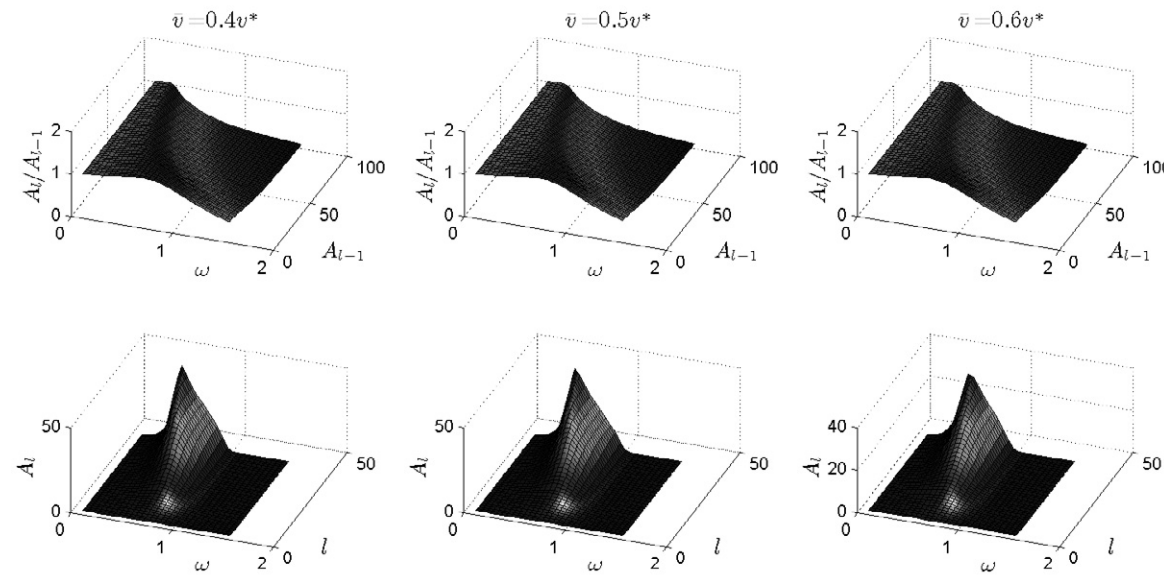

Figure 11: $\{R(A_{l-1},\omega)\}_{A_{l-1},\omega\in\mathbb{R}_+}$ and $\{A_l\}_{\omega\in\mathbb{R}_+,l=0,\cdots,L}$ surfaces for Case 4.

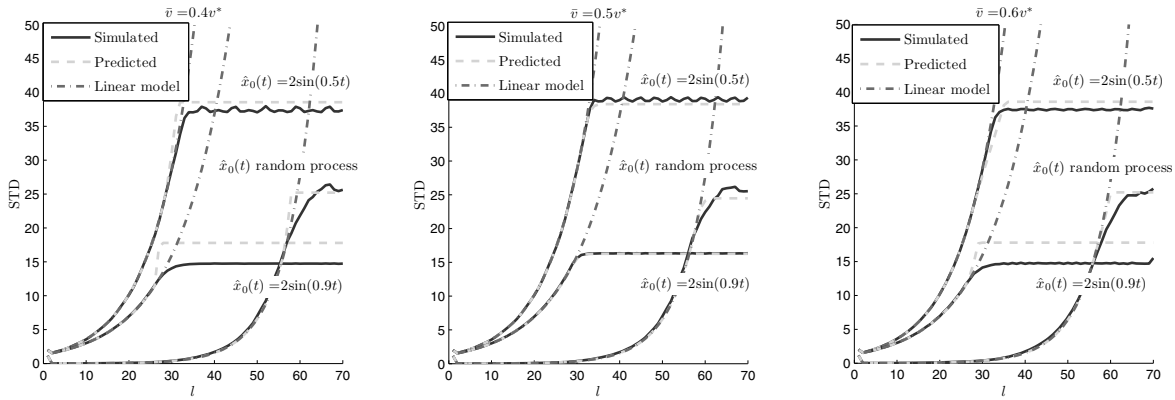

Figure 12: Prediction of oscillation propagation for Case 4.

5. Conclusion

This paper proposes a mathematical framework that is capable of characterizing traffic oscillation properties for a general class of car-following models, allowing for both linear and nonlinear dynamics. This framework starts with a new representation of car-following models using only oscillatory components in vehicle trajectories. A series of analytical methods to analyze local and asymptotic stabilities are discussed. In addition, we propose a novel systematic approach to quantify oscillation propagation period and magnitude across a platoon of vehicles for any given leading vehicle trajectory. Numerical experiments show that the proposed analysis framework can accurately quantify oscillation characteristics for a variety of car-following laws. In particular, our formulas can accurately analyze nonlinear car-following behavior and realistically predict the amplification of oscillation magnitude, while the traditional analysis based on linear models often leads to very unrealistic results. This proposed framework provides a global and quantitative perspective of the effects of nonlinearity on traffic oscillation's growth. It serves as a methodological basis for the design of dynamics models that are able to capture actual oscillation propagation mechanisms and reproduce empirically observed oscillation characteristics. Furthermore, this framework lays a solid foundation for future development of proper control strategies to effectively dampen oscillation amplification and mitigate traffic congestion.

This research can be extended in several directions. On the methodology side, this describing function technique can be extended to incorporate more frequency components in approximating an oscillatory process (see the harmonic balancing method in [46]). Such extension can possibly further enhance the accuracy of the predicted oscillation characteristics. The form of the car-following model may also be further generalized. For example, we can incorporate asymmetric driving behaviors and generalize function F_l into an asymmetric form [62]. This improvement is promising since the describing function method has been successfully used to quantify the oscillation response of an asymmetric nonlinear system [47]. On the application side, we are interested in applying this approach to empirical traffic data (e.g. NGSIM trajectory data), in the hope of using this framework to explain oscillation patterns observed in the field. The proposed framework may also serve as a building block to develop a guideline to map oscillation characteristics directly to the structures of nonlinear car-following models. With such a guideline, we may be able to effectively design or calibrate car-following models to reproduce any desired oscillation characteristics. This will possibly pave the foundation for developing effective countermeasures to traffic oscillations.

Acknowledgment

This research was supported in part by the National Science Foundation through Grant CMMI #0748067.

References

[1] M. Koshi, M. Iwasaki, I. Ohkura, Some findings and an overview on vehicular flow characteristics, in: V. Hurdle, E. Hauer, G. Stuart (Eds.), Proceedings of the 8th International Symposium on Transportation and Traffic Theory, 1983, pp. 403–451.
[2] R. D. Kuhne, Freeway speed distribution and acceleration noise, in: N. H. Gartner, N. H. Wilson (Eds.), Proceedings of the 10th International Symposium on Transportation and Traffic Theory, 1987, pp. 119–137.
[3] F. Paolo, The effect of driver behaviour on motorway reliability, Transportation Research Part B 23 (2) (1989) 139–150.
[4] B. Kerner, H. Rehborn, Experimental properties of complexity in traffic flow, Physical Review E 53 (5) (1996) R4275–R4278.
[5] B. S. Kerner, H. Rehborn, Experimental properties of phase transitions in traffic flow, Physical Review Letters 79 (20) (1997) 4030–4033.
[6] B. Kerner, Experimental features of self-organization in traffic flow, Physical Review Letter 81 (17) (1998) 3797–3800.
[7] D. Helbing, A. Hennecke, M. Treiber, Phase diagram of traffic states in the presence of inhomogeneities, Physical Review Letter 82 (21) (1999) 4360–4363.
[8] B. Kerner, Empirical macroscopic features of spatial-temporal traffic patterns at highway bottlenecks, Physical Review E 65 (4) (2002) 046138.
[9] L. Neubert, L. Santen, A. Schadschneider, M. Schreckenberg, Single-vehicle data of highway traffic: A statistical analysis, Physical Review E 60 (6) (1999) 6480–6490.
[10] M. Mauch, M. Cassidy, Freeway traffic oscillations: observations and predictions, in: M. A. Taylor (Ed.), Proceedings of the 15th International Symposium on Transportation and Traffic Theory, 2002, pp. 653–674.
[11] M. Treiber, D. Helbing, Reconstructing the spatio-temporal traffic dynamics from stationary detector data, Cooper@tive Tr@nsport@tion Dyn@mics 1 (2002) 3.1–3.24.
[12] X. Li, F. Peng, Y. Ouyang, Measurement and estimation of traffic oscillation properties, Transportation Research Part B 44 (1) (2010) 1–14.
[13] M. Cassidy, R. Bertini, Observations at a freeway bottleneck, in: A. Cedar (Ed.), Proceedings of the 14th International Symposium on Transportation and Traffic Theory, 1999, pp. 107–124.
[14] M. Cassidy, R. Bertini, Some traffic features at freeway bottlenecks, Transportation Research Part B 33 (1) (1999) 25–42.
[15] R. L. Bertini, M. T. Leal, Empirical study of traffic features at a freeway lane drop, Journal of Transportation Engineering 131 (6) (2005) 397–407.
[16] M. Cassidy, Increasing the capacity of an isolated merge by metering its on-ramp, Transportation Research Part B 39 (10) (2005) 896–913.
[17] M. Menendez, An analysis of HOV lanes: Their impact on traffic, Ph.D. thesis, University of California, Berkeley (2006).
[18] J. A. Laval, C. F. Daganzo, Lane-changing in traffic streams, Transportation Research Part B 40 (3) (2006) 251–264.
[19] J. Laval, M. Cassidy, C. Daganzo, Impacts of lane changes at merge bottlenecks: A theory and strategies to maximize capacity, in: Traffic and Granular Flow '05, 2007, pp. 577–586.
[20] S. Ahn, M. J. Cassidy, Freeway traffic oscillations and vehicle lane-change maneuvers, in: Transportation and Traffic Theory 2007, Vol. 1, Elsevier, 2007, pp. 691–710.
[21] W.-L. Jin, Y. Zhang, Paramics simulation of periodic oscillations caused by network geometry, Transportation Research Record 1934 (1) (2005) 188–196.
[22] R. E. Chandler, R. Herman, E. W. Montroll, Traffic dynamics: Studies in car following., Operations Research 6 (2) (1958) 165–184.
[23] R. Herman, E. W. Montroll, R. B. Potts, R. W. Rothery, Traffic dynamics: Analysis of stability in car following., Operations Research 7 (1) (1958) 86–106.
[24] D. C. Gazis, R. Herman, R. W. Rothery, Nonlinear follow-the-leader models of traffic flow., Operations Research 9 (4) (1961) p545–567.
[25] P. G. Gipps, A behavioural car-following model for computer simulation, Transportation Research Part B 15 (1981) 105–111.
[26] M. Bando, K. Hasebe, A. Nakayama, A. Shibata, Y. Sugiyama, Dynamical model of traffic congestion and numerical simulation, Physical Review E 51 (2) (1995) 1035–1042.
[27] M. Bando, K. Hasebe, K. Nakanishi, A. Nakayama, Analysis of optimal velocity model with explicit delay, Physical Review E 58 (5) (1998) 5429–5435.
[28] D. Helbing, B. Tilch, Generalized force model of traffic dynamics, Physical Review E 58 (1) (1998) 133–138.
[29] R. Jiang, Q. Wu, Z. Zhu, Full velocity difference model for a car-following theory, Physical Review E 64 (1) (2001) 017101.
[30] S. Sawada, Generalized optimal velocity model for traffic flow, International Journal of Modern Physics C 13 (1) (2002) 1–12.
[31] L. Davis, Modifications of the optimal velocity traffic model to include delay due to driver reaction time, Physica A 319 (2003) 557–567.
[32] X. Zhao, Z. Gao, A new car-following model: full velocity and acceleration difference model, European Physical Journal B 47 (1) (2005) 145–150.
[33] M. Treiber, A. Hennecke, D. Helbing, Congested traffic states in empirical observations and microscopic simulations, Physical Review E 62 (2) (2000) 1805–1824. doi:10.1103/PhysRevE.62.1805.
[34] D. Helbing, A. Hennecke, V. Shvetsov, M. Treiber, Micro- and macrosimulation of freeway traffic, Mathematical and Computer Modelling 35 (2002) 517.
[35] S. Hoogendoorn, R. Hoogendoorn, Calibration of microscopic traffic-flow models using multiple data sources, Philosophical Transactions of The Royal Society A 368 (1928) (2010) 4497–4517.
[36] A. Kesting, M. Treiber, D. Helbing, Enhanced intelligent driver model to access the impact of driving strategies on traffic capacity, Philosophical Transactions of The royal Society A 368 (1928) (2010) 45854605.
[37] S. Krauss, P. Wagner, C. Gawron, Metastable states in a microscopic model of traffic flow, Physical Review E 55 (5) (1997) 5597–5602.
[38] H. Y. Lee, H.-W. Lee, D. Kim, Origin of synchronized traffic flow on highways and its dynamic phase transitions, Physical Review Letters 81 (5) (1998) 1130–1133.
[39] Y. Igarashi, K. Itoh, K. Nakanishi, K. Ogura, K. Yokokawa, Bifurcation phenomena in the optimal velocity model for traffic flow, Physical Review E 64 (4) (2001) 047102.
[40] L. A. Safonov, E. Tomer, Y. Strygin, V. V.and Ashkenazy, S. Havlin, Multifractal chaotic attractors in a system of delay-differential equations modeling road traffic, Chaos 12 (4) (2002) 42–51.

[41] I. Gasser, G. Sirito, B. Werner, Bifurcation analysis of a class of car-following traffic models, Physica D 197 (3–4) (2004) 222241.
[42] G. Orosz, G. Stépán, Subcritical hopf bifurcations in a car-following model with reaction time delay, Proceedings of the Royal Society A 462 (2073) (2006) 26432670.
[43] D. Helbing, M. Moussaid, Analytical calculation of critical perturbation amplitudes and critical densities by non-linear stability analysis of a simple traffic flow model, The European Physical Journal B 69 (4) (2009) 571581.
[44] G. Orosz, R. E. Wilson, R. Szalai, G. Stpn, Exciting traffic jams: nonlinear phenomena behind traffic jam formation on highways, Physical Review E 197 (3) (2009) 222–241.
[45] G. Orosz, R. E. Wilson, G. Stépán, Traffic jams: dynamics and control, The Royal Society A 368 (1928) (2010) 4455–4479.
[46] A. I. Mees, Dynamics of Feedback Systems, John Wiley & Sons, Inc., New York, NY, USA, 1981.
[47] J.-J. Slotine, W. Li, Applied Nonlinear Control, Prentice Hall, 1990.
[48] C. Daganzo, Fundamentals of Transportation and Traffic Operations, Pergamon, 1997, Ch. Traffic Flow Theory, p. 155.
[49] Y. Ouyang, C. Daganzo, Characterization of the bullwhip effect in linear, time-invariant supply chains: some formulae and tests, Management Science 52 (10) (2006) 1544–1556.
[50] B. D. Greenshields, A study in highway capacity., in: Proc. Highw. Res. Board, 1934, pp. 448–477.
[51] G. F. Newell, A simplified theory of kinematic waves in highway traffic, part ii: Queueing at freeway bottlenecks, Transportation Research Part B 27 (4) (1993) 289 – 303.
[52] C. F. Daganzo, The cell transmission model: A dynamic representation of highway traffic consistent with the hydrodynamic theory, Transportation Research Part B 28 (4) (1994) 269 – 287.
[53] L. A. Pipes, An operational analysis of traffic dynamics, Journal of Applied Physics 24 (3) (1952) 274–281.
[54] G. F. Newell., Nonlinear effects in the dynamics of car following, Operations Research 9 (2) (1961) 209–229.
[55] M. J. Lighthill, G. B. Whitham, On Kinematic Waves. II. A Theory of Traffic Flow on Long Crowded Roads, Royal Society of London Proceedings Series A 229 (1955) 317–345.
[56] P. I. Richards, Shock Waves on the Highway , Operations Research 4 (1) (1956) 42–51.
[57] K. J. Astrom, R. M. Murray, Feedback Systems: An Introduction for Scientists and Engineers, Princeton University Press, 2008.
[58] B. Boashash, Time-Frequency Signal Analysis and Processing: A Comprehensive Reference, Oxford: Elsevier Science, 2003.
[59] G. F. Newell, A simplified car-following theory: a lower order model, Transportation Research Part B 36 (3) (2002) 195 – 205.
[60] J. Windover, M. Cassidy, Some observed details of freeway traffic evolution, Transportation Research Part A 35 (10) (2001) 881–894.
[61] J. A. Laval, L. Leclercq, A mechanism to describe the formation and propagation of stop-and-go waves in congested freeway traffic, Philosophical Transactions of the Royal Society A 368 (1928) (2010) 4519–4541.
[62] G. F. Newell, Instability in dense highway traffic, a review, in: J. Almond (Ed.), Proceedings of the second International Symposium on the Theory of Road Traffic Flow, Paris, 1965, pp. 73–83.

Appendix A. Proof for Proposition 1

Proof. Since $\mathbf{y}$ is an oscillatory series, let P denote its fundamental period. Then from Definition 1 we have $-\infty < y(t) = y(t+P) < +\infty, \forall t \in \mathbb{R}$ and $\int_0^P y(t) = 0$. Then there exist $y_-, y_+ \in \mathbb{R}$ such that $\min_{t\in\mathbb{R}} y(t) = y_-$ and $\max_{t\in\mathbb{R}} y(t) = y_+$. Since F is continuous and increasing, $\int_0^P [F(y(t)+s)]dt$ shall also be continuous and increasing with s. Sine F is strictly increasing in (a,c), $\int_0^P [F(y(t)+s)]dt$ shall be strictly increasing over $(a-y_+, c-y_-)$. It is obvious that $\int_0^P [F(y(t)+s)]dt \le PF(a) < PF(b)$ for any $s \le a-y_+$ and $\int_0^P [F(y(t)+s)]dt \ge PF(c) > PF(b)$ for any $s \ge c-y_-$. Thus there exists a unique $s^* \in (a-y_+, c-y_-)$ such that $\int_0^P [F(y(t)+s^*)]dt = PF(b)$, or $\int_0^P (F(y(t)+s^*) - F(b))dt = 0$. Also, it is obvious that $\{F(y(t)+s) - F(b)\}_{t\in\mathbb{R}}$ is bounded and has period P. Hence $\{F(y(t)+s) - F(b)\}_{t\in\mathbb{R}}$ is an oscillatory series. This completes the proof. □

Appendix B. Derivation of equation (11)

Property (ii) ensures that $|\mathcal{F}_l(A)| \in [0, K_l]$ for some K_l. Note that $\mathcal{F}_l(Ae^{j\phi}) = \mathcal{F}_l(A), \forall \phi \in \mathbb{R}$, and hence we can only use $\mathcal{F}_l(A)$ with $A \in \mathbb{R}_+$. The fundamental sinusoidal component equals

$$-A_l|\mathcal{F}_l(A_l)| \sin\left[\omega t + \phi_l + \angle(\mathcal{F}_l(A_l))\right]$$

where function $\angle(\cdot)$ gives the phase angle of a complex variable. From (10) we obtain

$$\{A_l \sin(\omega t + \phi_l)\}_{t\in\mathbb{R}} \approx \int \mathbf{G}_l \left[\{-A_l|\mathcal{F}_l(A_l)| \sin\left[\omega t + \phi_l + \angle(\mathcal{F}_l(A_l))\right]\}_{t\in\mathbb{R}}\right] dt. \tag{B.1}$$

The frequency domain representation of (B.1) is

$$A_l e^{j\phi} \approx \frac{\mathcal{G}_l(\omega)}{j\omega}\mathcal{F}_l(A_l)(-A_l)e^{j\phi}. \tag{B.2}$$

which yields

$$\mathcal{F}_l(A_l) - \frac{-j\omega}{\mathcal{G}_l(\omega)} \approx 0,$$

which is equation (11).